PERGAMON

Journal of South American Earth Sciences 16 (2003) 179–191

Journal of
South American
Earth Sciences

www.elsevier.com/locate/jsames

A kinematic model of the Scotia plate (SW Atlantic Ocean)

J.L. Giner-Robles[a], J.M. González-Casado[a,*], P. Gumiel[b], S. Martín-Velázquez[c], C. García-Cuevas[a]

[a]*Departamento de Química Agrícola, Geología y Geoquímica, Universidad Autónoma de Madrid, 28049 Madrid, Spain*
[b]*Instituto Geológico y Minero de España, 28003 Madrid, Spain*
[c]*Departamento de Geodinámica, Universidad Complutense de Madrid, 28040 Madrid, Spain*

Received 30 November 2001; accepted 31 January 2003

Abstract

The focal mechanisms located around the Scotia plate were examined by fault population analysis to calculate both the trends of the maximum horizontal shortening on the plate and the orientations of its associated faults. The results show that both the northern and southern boundaries of the Scotia plate (the north and south Scotia ridges) are currently undergoing left-lateral movement. This movement induces a left-lateral shear couple in the whole plate, with a maximum horizontal NE–SW shortening direction. The established fault orientations and fault classes closely match the predicted structural pattern of a theoretical shear couple that includes the entire Scotia plate. The stress trajectories deduced from finite element modeling also agree with the proposed left-lateral shear couple model; the calculated stress trajectories are characterized by a homogeneous NE–SW compression direction over the whole Scotia plate. This shear model also explains the slip of recent tectonic structures found at the boundaries of the Scotia plate and suggests the possibility of reactivation of its former tectonic structures.

Keywords: Focal mechanisms; Plate kinematics; Plate tectonics; Scotia plate; Scotia sea

1. Introduction

This work analyzes the current plate kinematics of the Scotia Sea region. Local earthquake focal mechanisms were selected from the Harvard Centroid Moment Tensor Catalog (CMT) and examined by fault population analysis (right dihedra method, Angelier and Mechler, 1977; slip model, Reches, 1983; De Vicente, 1988), which enabled us to calculate the orientation of the maximum horizontal shortening (e_{HMAX}). It also established the nodal plane corresponding to the fault that caused these seismic events. Galindo-Zaldivar et al. (1996) and González-Casado et al. (2000) previously have used this method to determine the characteristics of recent deformation of a small part of the Scotia Sea region (the Bransfield basin). Our analysis of the entire Scotia Sea region provides the basis for an elastic finite element analysis to model the stresses throughout the Scotia plate. Using the deduced stress orientations and observed tectonic structures, we propose a kinematic model for this plate.

2. Geological setting

The Scotia plate, a small tectonic plate located in the Scotia Sea region and made up of oceanic lithosphere and small continental fragments, extends from approximately 50–63°S and 70–20°W (southwestern Atlantic) (Fig. 1). The tectonic development of this plate began 40 M years ago, when the continental fragments now distributed around the Scotia Sea (Fig. 1) were joined at an active subducting Pacific margin to form a continuous landmass from the Antarctic Peninsula to South America (Barker and Burrell, 1977; Barker, 1995, 2001). Barker (2001) indicates that a second subduction system, an eastward convex arc, was located on the Atlantic margin of this land bridge. The backarc extension behind this theoretical east-migrating subduction zone would have produced the Scotia Sea and driven the continental fragments eastward until they reached their current position (for a detailed description of

* Corresponding author.
E-mail addresses: g.casado@uam.es (J.M. González-Casado), jorge.giner@uam.es (J.L. Giner-Robles).

0895-9811/03/$ - see front matter © 2003 Elsevier Ltd. All rights reserved.
doi:10.1016/S0895-9811(03)00064-6

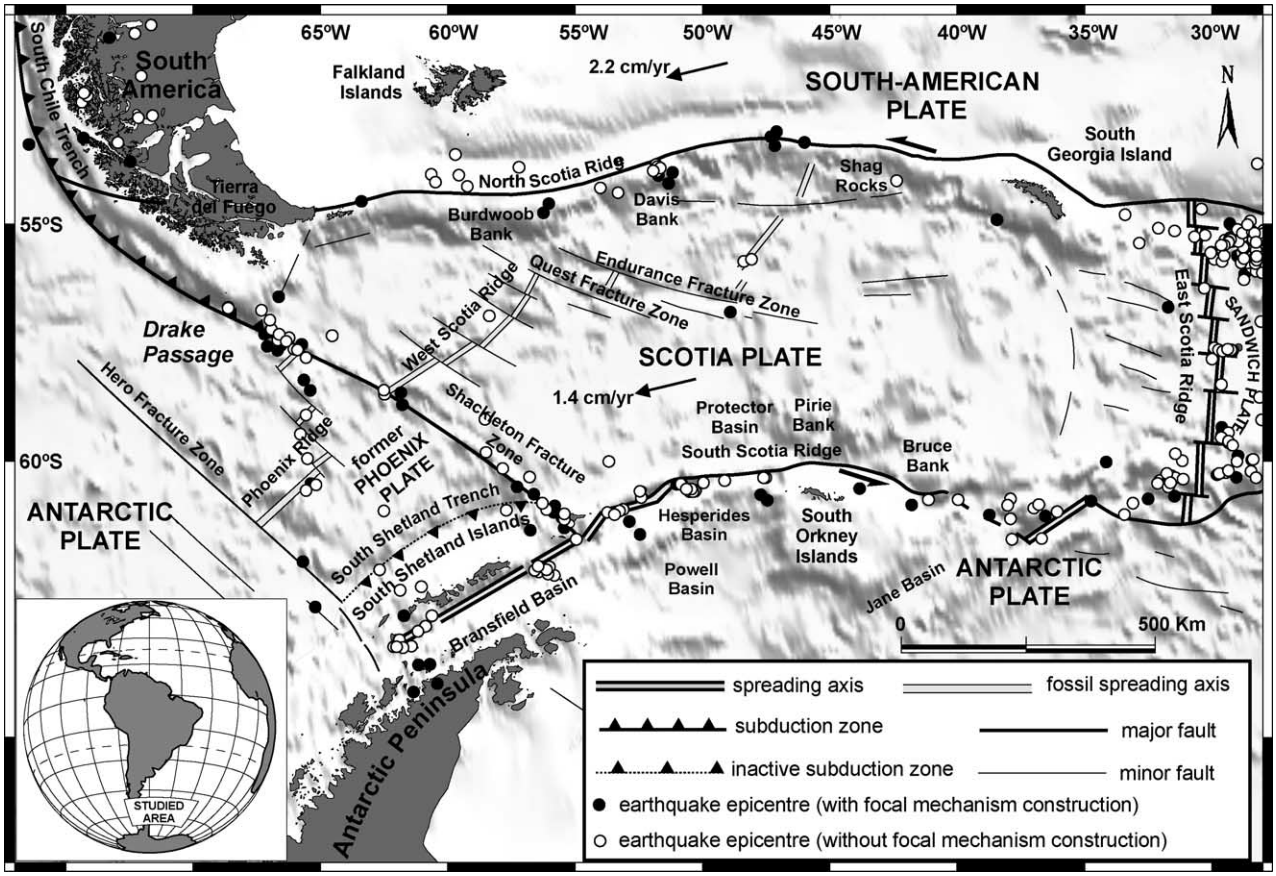

Fig. 1. Tectonic diagram of the main geological structures and plate boundaries in the Scotia Arc and Antarctic Peninsula (modified from Tectonic map of the Scotia Arc (1985), Pelayo and Wiens (1989), Galindo-Zaldivar et al. (1996) and Gràcia et al. (1996)). Locations of earthquake epicenters are from the Engdahl Catalog (Engdahl et al., 1988). White circles indicate events without construction of the focal mechanisms; black circles indicate events with construction of the focal mechanisms (from Pelayo and Wiens, 1989; CMT). The slip motion vectors are from Pelayo and Wiens (1989).

the development of the Scotia Sea region, see Barker, 2001). In this paper, the Scotia Sea region is considered to consist of two small plates, Scotia and Sandwich, surrounded by the major Antarctic and South American plates (Tectonic map of the Scotia Arc, 1985) (Fig. 1).

The modern Scotia plate is a roughly rhomboid fragment 800 km wide and 3000 km long (Fig. 1) with two pairs of E–W and N–S boundaries that exhibit different tectonic development and characteristics. The boundaries between the Scotia plate and the Antarctic and South American plates have a roughly E–W trend, and at present, both show sinistral strike–slip motion (Forsyth, 1975; Pelayo and Wiens, 1989; Livermore et al., 1994) (Fig. 1). Several small, linear troughs (pull-apart basins), such as the Hesperides Deep (Acosta and Uchupi, 1996); the extensional offset in the Scotia–Antarctic plate boundary at around 51°W (Barker, 2001); the sedimentary basins in the southern part of South Orkney Island; and other tectonic elements along the southern boundary suggest a recent transtensional tectonic regime for the south Scotia ridge (Forsyth, 1975; Pelayo and Wiens, 1989; Barker et al., 1991; Galindo-Zaldivar et al., 1994; Klepeis and Lawver, 1996). In contrast, the north Scotia ridge contains an almost continuous line of small, continental, lithospheric fragments (the Tierra del Fuego block, the Burdwood, the Davis and Aurora banks, and the south Georgia block) that evince compressional deformation during at least the last 7 Ma (Cunninghan et al., 1998). These data suggest that the boundary has a transpressive character (Forsyth, 1975; Pelayo and Wiens, 1989; Barker et al., 1991; Cunninghan et al., 1998). Pelayo and Wiens (1989) propose a left-lateral motion for these boundaries (north Scotia ridge 0.5 cm/y; south Scotia ridge 1 cm/y). In an absolute reference frame (Gordon et al., 1988), the Scotia plate motion is toward the WSW (2.2 cm/y), and the Sandwich plate is moving rapidly toward the east (5.5 cm/y) (Pelayo and Wiens, 1989). The NW–SE-trending Shackleton fracture zone (SFZ) is the western boundary that separates the Scotia plate from the Antarctic and former Phoenix plates. This boundary shows a general transpressive character in its southeastern section (Klepeis and Lawver, 1996; González-Casado et al., 2000). In the northwestern section, there is likely some oblique subduction of the Antarctic plate's oceanic crust beneath the continental lithosphere of the northwestern tip of the Scotia plate (Maldonado et al., 2000). To the east, the Scotia plate is separated from the Sandwich plate by the east Scotia ridge, a N–S-trending ridge marked by prominent topographic and gravity highs (Barker, 1995). This

intermediate-stage backarc spreading ridge is an effect of subduction at the south Sandwich trench (Fig. 1). The Sandwich plate traditionally has been studied together with the Scotia plate because its northern and southern limits are eastward extensions of the north and south Scotia ridges (Fig. 1). However, its eastern boundary is a deep-ocean trench (the south Sandwich trench) that accommodates convergence with the South American plate and gives rise to an active volcanic arc on the Sandwich plate.

Details of the current relative plate motions around the Scotia Sea region are poorly understood, and various tectonic models have been proposed for both the entire plate and some of its boundaries (Barker, 1970; Forsyth, 1975; Herron et al., 1977; Pelayo and Wiens, 1989; Klepeis and Lawver, 1996; Galindo-Zaldivar et al., 1996; Cunninghan et al., 1998; González-Casado et al., 2000; Barker, 2001). The variation in the models proposed is due to a lack of precise information about the characteristics of many submarine structures and scarce seismological and structural data in some models. The Scotia Sea region as a whole displays moderate seismic activity; in the last 34 years, more than 426 seismic events with magnitude ≥ 4.0 mb have occurred (Fig. 1). The main seismic activity of the plate is associated with the south Sandwich subduction zone. Seismic data have been used in previous investigations to establish the principal stress orientations and discuss the activity of these plate boundaries (Forsyth, 1975; Pelayo and Wiens, 1989; Cunninghan et al., 1998), and several papers have focused on the smaller Bransfield Strait region (Galindo-Zaldivar et al., 1996; Klepeis and Lawver, 1996; González-Casado et al., 2000).

3. Method

3.1. Right dihedra method

The right dihedra method (Angelier and Mechler, 1977) determines common zones of compression and tension for a set of focal mechanisms. The orientation of the compression (P) and tension (T) axes, located in the area of maximum tension and compression, coincide approximately with the orientations of the main axes of the strain ellipsoid (e_y = maximum shortening direction; e_x = maximum extension direction). Several right dihedra diagrams were calculated using CMT focal mechanism data. The three-dimensional orientation of the P/T zones in stereographic projection enables deduction of the tectonic regime (i.e. whether deformation is related to convergence, divergence, or passive tectonic processes), as well as the orientations of the maximum horizontal extension (e_{HMIN}) and maximum horizontal shortening (e_{HMAX}). Several authors have successfully used this method in other tectonic realms (Gephart and Forsyth, 1984; Harmsen and Rogers, 1986; Michael, 1984; Rivera and Cisternas, 1990; Capote et al., 1991; Bergerat and Angelier, 2000). However, it is not ideal because it allows for multiple interpretations of diagrams in tectonically heterogeneous regions.

3.2. Slip model

A more accurate determination of the main shortening and extension directions associated with a seismic episode requires the use of fault population analysis methods (Reches, 1983). However, these can only be used if the fault plane, of the two nodal planes defining the focal mechanisms, is known, as well as the slip direction of the selected fault plane. The data from the CMT used for this analysis were the orientations of the two nodal planes and their respective slip vectors. To determine which nodal plane was the active fault plane, both planes were plotted on a pitch–dip diagram (Capote et al., 1991). In this diagram, four fields of relationships among fault dips, striation pitches, classes of strain ellipsoid ($K' = e_y/e_x$), and the internal friction angle are set. Each focal mechanism yields two possible faults and their corresponding dip and pitch. Thus, each nodal plane is located in one of the four fields of the pitch–dip diagram (strike–slip normal, normal strike–slip, strike–slip reverse, and reverse strike–slip), and its normal or reverse character can be established—though only one is a real fault. We chose a fault plane whose normal or reverse character was the same as its focal mechanism character, namely, the tectonic regime (for a detailed description of this method, see De Vicente (1988) and Capote et al. (1991)). Finally, the orientation of the maximum horizontal shortening (e_{HMAX}) was determined for each fault using the equations proposed by De Vicente (1988) and Capote et al. (1991) and based on the Reches slip model. This technique has been used by other authors (De Vicente et al., 1996; Giner-Robles, 1996; González-Casado et al., 2000; Herraiz et al., 1996, 2000) with adequate results. This procedure was used for all the CMT focal mechanisms believed to establish the fault and e_{HMAX} orientations of the Scotia plate (Table 1). Earthquakes were sorted by their geographical proximity and association with known tectonic structures.

The use of two independent analysis methods enables us to evaluate the validity of the adopted fault plane. If the results from both methodologies are similar, the fault planes have been correctly determined.

3.3. Finite element model

Tectonic stress orientations for the Scotia plate were predicted using two-dimensional plane-stress elastic finite element analysis, assuming an elastic mechanical behavior and the stress sources as pressures (surface force loads). The values of Young's modulus and the Poisson coefficient were assigned according to the Scotia plate's geological characteristics. Calculations were performed using the ANSYS finite element package (Swanson Analysis System, Inc.). This method is based on the division of a surface into small

Table 1
Parameters of the earthquake chosen for the study of the present strain state

Event	Date	Origin time GMT	Lat	Long	Depth	mb	Fault plane			Fault character	e_{HMAX}	Zone
							dd	d	p			
1	06/04/62	19:00:11.0	−60	−33.7	8		103	65	106	N	20	B3
2	26/09/65	21:33:54.0	−54.8	−38.3	7	6.1	58	30	89	R	57	Intraplate
3	27/09/69	09:04:03.0	−60.9	−56	7	5.8	27	79	178	OR	117	C1
4	15/06/70	11:14:52.0	−54.3	−63.6	6	5.6	269	87	168	ON	13	A
5	08/02/71	21:04:22.0	−63.5	−61.2	15	6.3	340	50	84	N	66	F
6	25/02/73	05:35:55.0	−61	−37.9	24	6.4	285	79	163	ON	47	B2
7	29/12/75	03:39:43.0	−56.8	−68.5	11	6.1	77	15	89	R	76	D1
8	14/02/76	03:10:37.0	−57.4	−64.4	9	6	54	40	118	R	76	D1
9	05/08/78	06:43:15.9	−60.84	−56.37	15	5.8	227	64	162	OR	100	C1
10	22/05/79	21:38:30.6	−60.84	−31.95	15	5.1	310	67	107	N	47	B3
11	06/06/79	10:54:26.6	−53.93	−74.65	15	5.5	97	8	76	R	83	E
12	23/09/79	22:43:41.8	−60.61	−50.75	15	5.9	117	49	116	N	45	B1
13	07/11/79	11:31:50.3	−62.56	−72.81	15	5.1	83	48	59	R	61	G
14	07/11/79	14:03:50.2	−60.77	−41.74	15	5.2	183	90	0	SS	93	B1
15	05/02/80	13:52:52.9	−57.42	−66.69	15	5.2	30	41	123	R	56	D1
16	15/09/80	04:28:17.4	−61.25	−56.85	32	5.8	141	76	86	N	59	C
17	18/01/81	03:06:50.7	−61.05	−55.55	28.4	6	123	26	87	R	120	C1
18	27/03/81	22:02:33.9	−59.57	−31.35	15	5.1	246	89	177	ON	174	B3
19	09/11/81	22:56:52.0	−61.75	−65.26	15	5.1	265	90	0	SS	40	G
20	21/03/82	15:55:14.9	−52.66	−47.12	15	5.4	267	90	0	SS	42	A1
21	25/03/82	05:05:39.8	−52.97	−45.89	10	5.9	176	75	178	OR	78	A1
22	30/03/82	04:24:34.5	−52.9	−47.41	15	5.2	284	90	0	SS	59	A1
23	11/09/82	23:55:11.5	−58.54	−61.73	15	5.2	261	90	0	OR	36	D2
24	18/11/82	00:27:54.8	−54.59	−55.63	10.1	5.6	237	9	97	R	64	A3
25	19/11/82	10:57:37.7	−54.81	−55.85	10.1	5.5	285	12	40	R	56	A3
26	12/12/82	19:57:34.4	−63.76	−60.98	15	5.5	105	53	123	N	36	F
27	13/12/82	02:50:58.0	−64.02	−60.35	11.2	5.7	323	60	80	N	48	F
28	22/01/83	11:37:07.9	−62.56	−64.76	10	5.5	327	68	91	N	57	G
29	12/05/83	02:55:03.1	−58.65	−61.81	15	5.3	281	90	0	SS	56	D2
30	11/07/83	12:56:41.4	−60.99	−52.57	13.6	6.1	347	69	32	ON	47	B1
31	09/01/84	13:43:28.4	−61.19	−34.77	10	5.5	310	66	97	N	43	B2
32	30/03/84	16:40:17.8	−62.68	−61.81	41.2	5.5	5	47	169	OR	79	F
33	04/05/84	17:36:59.0	−58.3	−65.02	10	5.5	117	83	156	ON	42	D2
34	13/09/86	09:28:30.8	−61.11	−36.46	15	5.8	280	87	170	ON	27	B2
35	22/12/86	14:18:45.0	−57.1	−49.05	15	6	194	84	29	ON	93	Intraplate
36	20/05/87	13:54:18.6	−61.38	−52.37	15	5.5	314	50	102	N	52	B1
37	14/06/87	18:22:17.9	−58.47	−64.83	15	5.1	284	90	0	SS	59	D2
38	21/06/87	10:09:01.9	−57.56	−66.9	15	5.4	257	90	0	SS	32	D2
39	03/11/88	17:15:52.1	−60.79	−56.04	15	5.1	225	14	151	R	105	C1
40	16/03/89	07:24:02.0	−63.96	−61.41	15	5.3	15	79	84	N	104	F
41	12/09/90	20:16:24.7	−60.47	−65.29	15	5.5	281	75	10	OR	45	G
42	06/03/91	13:08:10.0	−57.22	−66.38	15	5.1	279	79	11	OR	55	D2
43	24/05/91	18:28:41.4	−60.38	−44.39	15	5.4	197	33	154	OR	77	B2
44	17/06/92	08:39:20.0	−60.49	−57.35	15	5.8	302	87	170	ON	49	C2
45	14/07/92	22:24:21.9	−57.13	−30.64	20.5	5.1	279	75	141	ON	27	Intraplate
46	30/07/92	13:14:57.4	−51.12	−72.59	15	5.4	121	25	66	R	99	E
47	01/10/92	03:21:12.1	−53.63	−51.48	15	5.3	245	90	0	SS	20	A2
48	01/10/92	18:15:48.2	−54	−51.38	15	5.4	250	81	150	ON	175	A2
49	12/11/92	15:00:47.2	−53.69	−51.61	15	5.8	244	90	0	SS	19	A2
50	23/06/93	11:29:24.2	−60.59	−56.76	15	5.6	306	88	169	ON	46	C2
51	27/09/93	13:37:39.8	−53.77	−51.08	17.3	6.1	267	87	123	ON	179	A2
52	03/01/95	16:12:00.7	−56.67	−66.42	16	6.1	205	45	124	R	50	D1
53	30/05/95	16:56:26.5	−60.42	−30.94	15	5.2	279	66	136	N	32	B3
54	06/04/96	12:17:35.1	−53.39	−77.26	15	5.1	256	27	61	R	50	E
55	31/08/96	18:59:20.6	−53.43	−73.12	30.2	5.1	134	77	148	ON	64	E
56	15/11/98	13:27:12.8	−60.86	−47.3	15	5.3	305	61	103	N	41	B1
57	09/06/99	04:05:48.9	−53.2	−47.41	15	5.4	177	20	157	OR	63	A1

Hypocentral parameters: date, hour (GMT), location (Lat–Long), depth (km), and magnitude (mb). Parameters calculated in this study: orientation of the fault plate deduced from the focal mechanism (dip) and the slip direction (pitch), fault character (R, reverse fault N, normal fault; ON, oblique-normal fault; OR, oblique-reverse fault; SS, strike–slip fault), maximum horizontal shortening (e_{HMAX}), and zone (see Fig. 4).

units, that is, elements related to one another by nodes. Each element is allowed a different mechanical behavior, and on the basis of the node displacement, the deformation inside each finite element is established (Zienkiewicz and Taylor, 1994). Because a model is always a simplification of reality, the general objective of our model is to determine whether the stress orientation deduced from focal mechanisms fits the proposed Scotia plate kinematic model. Previous works confirm the usefulness of this approach in modeling intraplate stress fields (Cloetingh and Wortel, 1986; Richardson and Reding, 1991; Meijer et al., 1997; Coblentz et al., 1995, 1998) and paleostress fields deduced from fault-slip data (Muñoz-Martín et al., 1998).

4. Results

4.1. Earthquake focal mechanism analysis

Between 1964 and 1998, there were 426 earthquakes with magnitudes between 4.0 and 6.3 in the Scotia Sea region (Engdahl Catalog; Engdahl et al., 1988). Fifty-seven

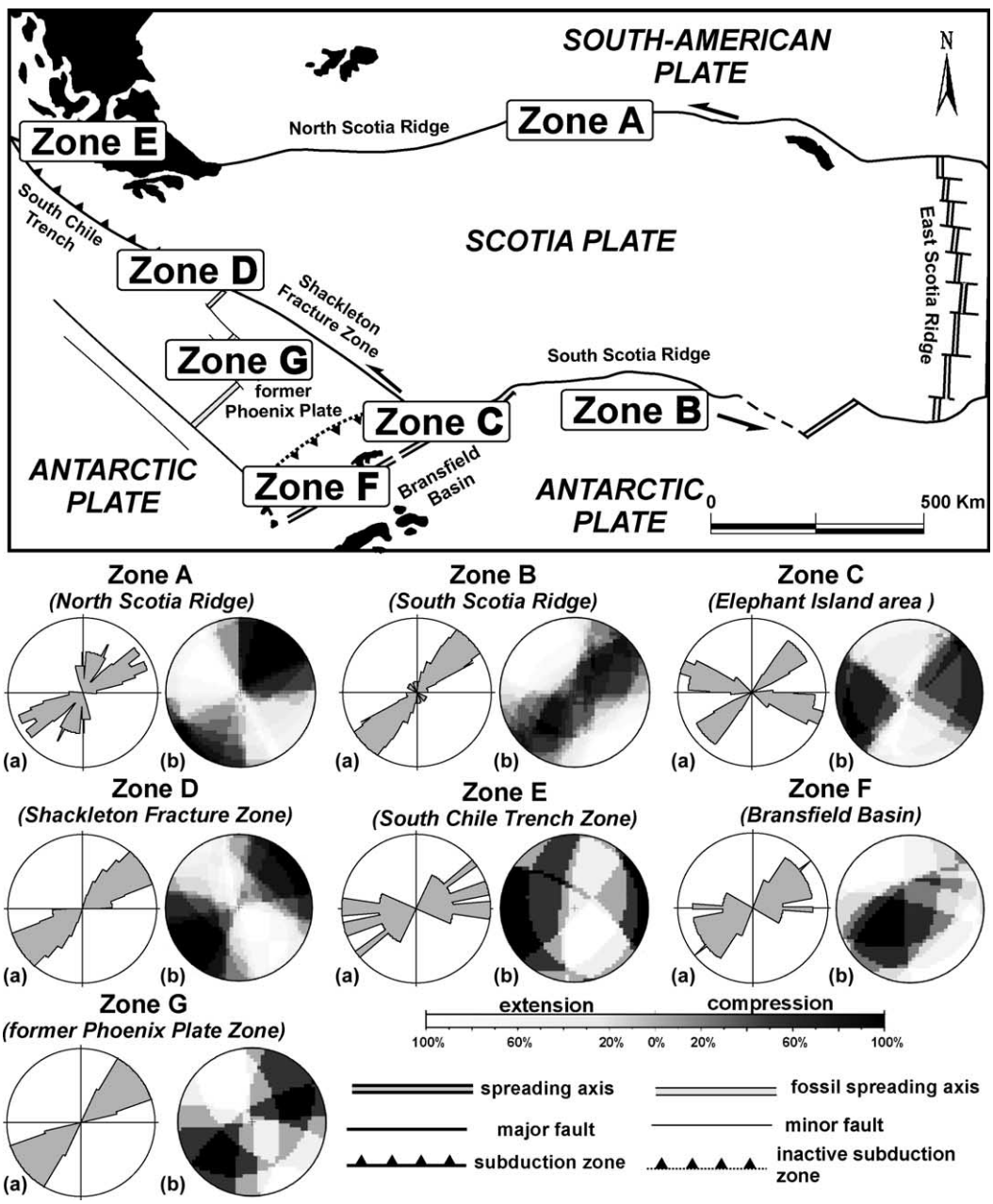

Fig. 2. Results from the analysis of the earthquake focal mechanisms using the right dihedra method (Angelier and Mechler, 1977) and the slip model (Reches, 1983; De Vicente, 1988). The focal mechanisms have been grouped for analysis on the basis of their geographical proximity to the main geological structures. The results from each zone are represented by (a) rose diagrams of maximum horizontal shortening orientation (e_{HMAX}) using the slip model (the circle corresponds to values of 50%) and (b) right dihedra diagrams.

earthquakes with ≥5.0 mb were used for the data set; 44 were near the plate boundaries, and 13 were along the prolongation of these structures on the surrounding plates (Fig. 1). Of the 57 focal mechanisms analyzed, 50 solutions were obtained from the Harvard CMT (Dziewonski et al., 1981; Dziewonski and Woodhouse, 1983). The other seven focal mechanisms for events between 1962 and 1975 were taken from Pelayo and Wiens (1989).

To perform the analysis, the earthquakes were grouped according to their geographical proximity to the major plate boundaries (Fig. 2). The focal mechanisms located within the Scotia plate (three events) were very isolated and could not be grouped for meaningful results.

4.1.1. The northern and southern boundaries

Both boundaries yield NE–SW e_{HMAX} orientations, ca. 45° offset from the ridge trends (Fig. 2). This orientation is consistent with the proposed left-lateral strike–slip movement (Forsyth, 1975; Pelayo and Wiens, 1989; Barker et al., 1991; Livermore et al., 1994; Klepeis and Lawver, 1996). The shortening directions are consistent with a westward movement of the Scotia plate. However, the fault type associated with the individual focal mechanisms varied from north to south. At the south Scotia ridge (Zone B, 13 events; Fig. 2), dip–slip and normal-oblique faults prevailed, whereas at the north Scotia ridge (Zone A, 11 events; Fig. 2), strike–slip and reverse-oblique faults dominated. These mechanisms coincide with the proposed transtensional and transpressional tectonic regimes for the south and north Scotia ridges, respectively.

4.1.2. The western boundary

At the SFZ (Zone D; Fig. 2), the e_{HMAX} is nearly orthogonal to the trend of the structure. In this region, most focal mechanisms are oblique or reverse. Considering the westward movement of the Scotia plate relative to the Antarctic plate, the tectonic character of this boundary must be more compressive than passive. At the south Chile trench zone (Zone E, 4 events; Fig. 2), e_{HMAX} rose orientations (slip model) and right dihedra diagrams both show the e_{HMAX} is orthogonal to the principal orientation of this structure, where a convergent boundary is well established. Thus, the two tectonic structures correspond to a convergent tectonic margin, and the northwestern limit of the Scotia plate is characterized by a compressional tectonic regime related to subduction of the Antarctic plate under the South American plate at the south Chile trench. At the corner of the Scotia plate close to the South Shetland Islands region (Zone C, 7 events; Fig. 2), seismicity seems concentrated at the intersection of the SFZ and the south Scotia ridge (Fig. 1). The synthetic right dihedra diagram shows the e_{HMAX} trends ENE–WSW and is characteristic of a wrench tectonic regime. The two theoretical strike–slip fault planes deduced from this diagram are subvertical and subparallel to the SFZ and the south Scotia ridge. The e_{HMAX} rose orientation (slip model) shows two modes of orientation: one parallel to the predominant NE–SW orientation deduced for the rest of the region, and the other WNW–ESE, which might represent local deformation near Elephant Island where the Bransfield basin and the south Shetland trench connect with the Scotia plate.

4.1.3. The eastern boundary

At the boundary between the Scotia and south Sandwich plates, the seismic magnitudes are smaller (<5 mb), and CMT solutions were not possible. In contrast, at the south Sandwich trench, there were many earthquakes with magnitudes >5 mb but with deep hypocenters related to the subduction of the South American plate beneath the south Sandwich plate. Therefore, the only events used were those with a hypocentral depth of less than 50 km. The results show an e_{HMAX} orientation trending approximately ENE–WSW.

4.1.4. The former Phoenix plate/Bransfield basin region

In the Bransfield basin (Zone F, 5 events; Fig. 2), the results show an e_{HMAX} trending NE–SW. The right dihedra diagram is characteristic of an extensional tectonic regime. These results resemble, in both maximum horizontal shortening and associated fault type, those deduced for the south Scotia ridge. In the neighboring former Phoenix plate (Zone G, 4 events; Fig. 2), the diagrams show a NE–SW e_{HMAX} orientation. The seismicity of the Phoenix plate was dispersed and showed no apparent relationship to the main geological structures. The only observable trend is that modern earthquakes seem to be located at the N and W limits of the former Phoenix plate. This plate is currently considered part of the Antarctic plate (Barker and Dalziel, 1983; Pelayo and Wiens, 1989; Larter and Barker, 1991; Maldonado et al., 1994).

To further characterize Scotia plate deformation, the orientation of e_{HMAX} was calculated for each of the nodal planes favored by the slip model (Fig. 3). For normal faults, the maximum horizontal extension (e_{HMIN}) was considered. These new data were grouped by both geographical proximity and the focal mechanism to be analyzed (Fig. 4). Because the main objective of this work is to determine present deformation of the Scotia plate, this detailed analysis was performed mainly at the boundaries of the plate. Right dihedra diagrams from the fault analysis for each of the new data groups (Fig. 4) provide more accurate pictures of the tectonic regime associated with each zone to be established.

4.1.5. The north Scotia ridge

Along this boundary, there are three seismicity groups, each with a unique focal mechanism character (Zones A1–A3; Fig. 4). Strike–slip and oblique-reverse faults characterize the north Scotia ridge east zone (Zone A1, 4 events), strike–slip and oblique-normal faults characterize the north Scotia ridge central zone (Zone A2, 4 events), and reverse faults characterize the north Scotia ridge west zone (Zone

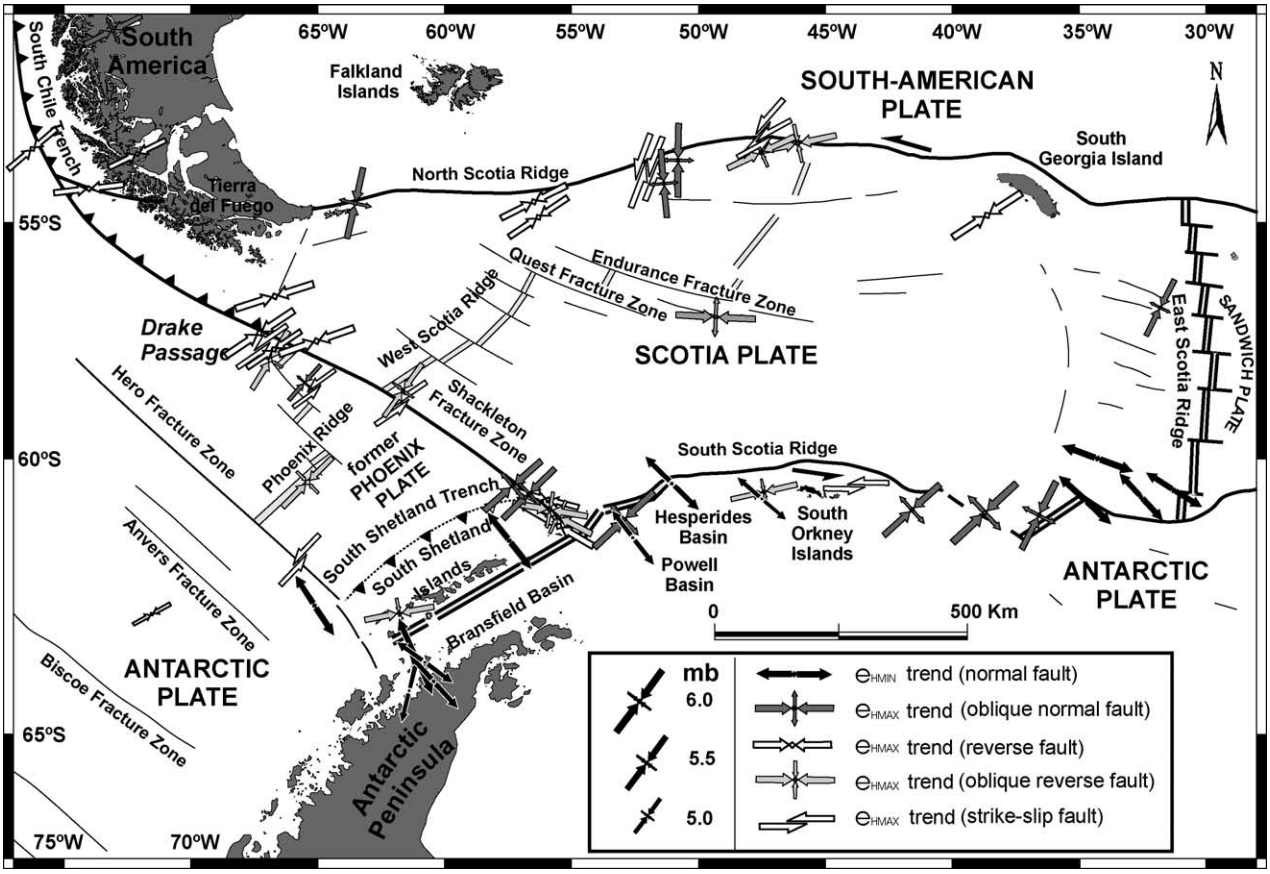

Fig. 3. e_{HMAX} orientations for each focal mechanism using the slip model (Reches, 1983; De Vicente, 1988). The orientation of the e_{HMAX} is defined by the arrow. For normal faults, the orientation of e_{HMIN} is shown. Tectonic symbols are as in Fig. 1.

A3, 2 events). An isolated earthquake to the west of the north Scotia ridge (Fig. 3) was not considered in the classification. The north Scotia ridge thus exhibits a change from a compressional regime near the south Chile trench (Zone E; Fig. 2) and in Zone A3 (Fig. 4) to a strike–slip regime further east (Zones A2 and A1). A similar development scheme has been proposed by Cunninghan et al. (1998).

4.1.6. The south Scotia ridge

Seismicity along the south Scotia ridge (Zones B1–B3; Fig. 4) was subdivided into three geographical areas with similar seismic characteristics: the south Scotia ridge west zone (Zone B1, 5 events), which included all earthquakes located west of the South Orkney Islands; the south Scotia ridge central zone (Zone B2, 4 events), including all earthquakes located near this fracture zone east of the South Orkney Islands; and the south Scotia ridge east zone (Zone B3, 4 events), which included all events between Discovery bank and the east Scotia ridge. The right dihedra diagrams show alternating zones of strike–slip tectonics and extensional tectonics (e.g. Acosta and Uchupi, 1996), consistent with the pull-apart basins and transtensional character of this boundary. Coincidentally, the alternate tectonic regimes seem to continue beyond the Scotia plate and into the Bransfield basin (Zone F; Fig. 2), where a maximum horizontal shortening similar to that of the south Scotia ridge appears. However, the orientation of the e_{HMAX} shows no meaningful variation, which may suggest a single, global tectonic process.

4.1.7. The southwestern corner

The corner of the Scotia plate close to the South Shetland Islands area (Zones C1 and C2; Fig. 4) is tectonically complex. The data for this area were grouped into two populations according to fault type and earthquake locations relative to the principal plate boundaries and by maximum horizontal shortening orientation. Zone C1 includes earthquakes associated with reverse faults near the northeastern end of the south Shetland archipelago (Elephant Island), south of the south Shetland trench. From the analysis of the seismic data (four events), a N95°E e_{HMAX} orientation is deduced, defined by reverse and oblique-reverse faults. This orientation is very different from others obtained at the Scotia plate limits and may be interpreted as the result of the extension produced in the Bransfield basin, which would cause a local compressive stress field in the northern part of the area subject to extension (González-Casado et al., 2000). Zone C2 is defined by two events located at the SFZ, north of the south Shetland trench. The results of the analysis of

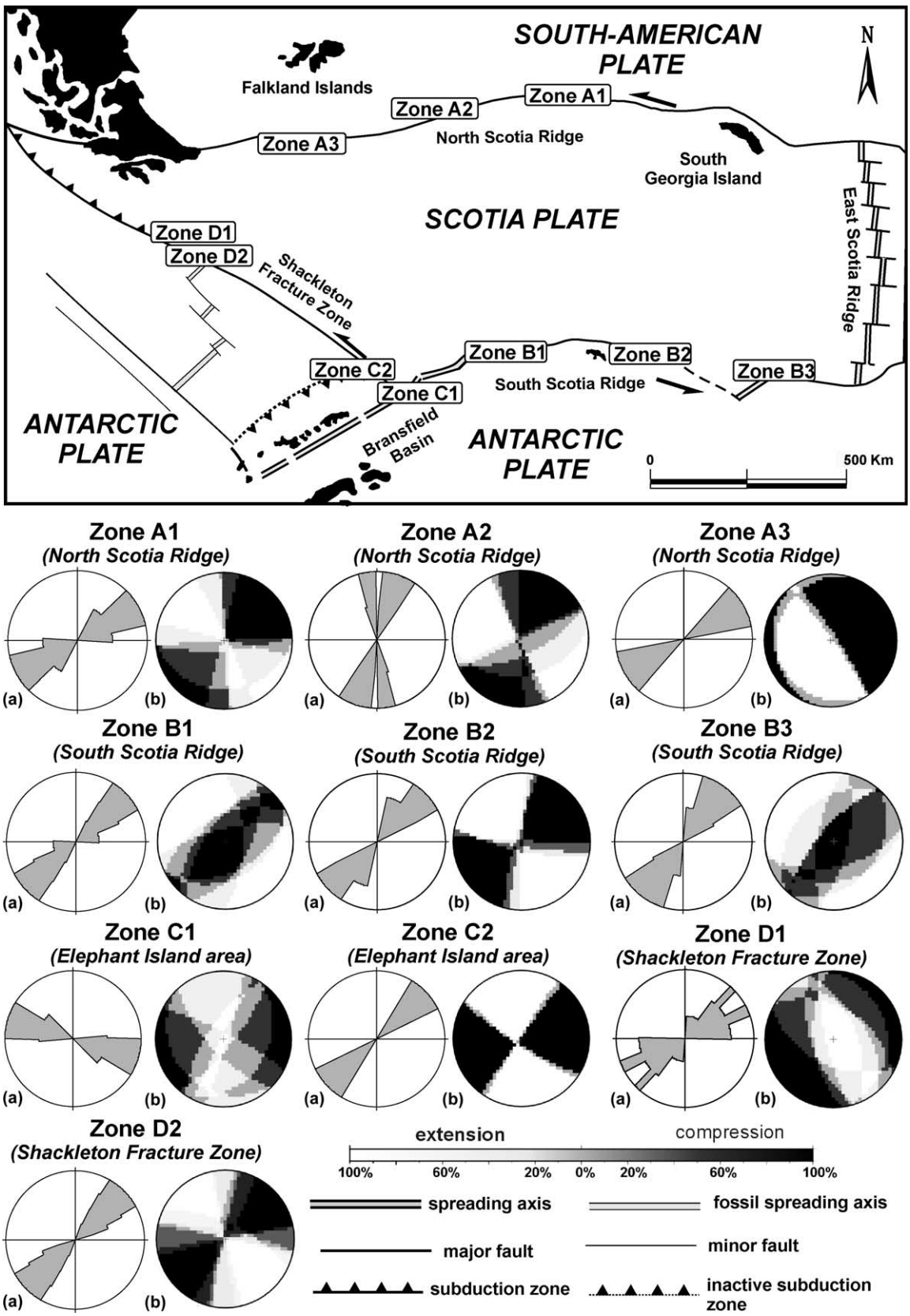

Fig. 4. Results from the analysis of the focal mechanisms using the right dihedra method (Angelier and Mechler, 1977) and the slip model (Reches, 1983; De Vicente, 1988) for the new groups with earthquakes classified by both geographical proximity and fault type. The results from each zone are represented by (a) rose diagrams of e_{HMAX} deduced from the slip model (the circle corresponds to the 50%) and (b) right dihedra diagrams.

these earthquakes (Zone C2; Fig. 4) show an e_{HMAX} trending N55°E. This orientation, as well as the faults related to the focal mechanisms, seems related to convergent deformation in the NW zone of the SFZ (Zone D2; Fig. 4) instead of the nearby earthquakes located in Zone C1.

4.1.8. The western boundary

The SFZ (Zone D, 10 events) was subdivided into two areas: the Shackleton fracture north zone (Zone D1, 4 events) and the Shackleton fracture central zone (Zone D2, 6 events). No meaningful variation in the deduced orientations of the maximum horizontal shortening (NE–SW) existed in these zones, but a spatial variation in the type of tectonic regime along this limit was well defined as changing from compression (Zone NW) to strike–slip (Zone SE; Fig. 4).

4.2. Stress modeling results

To model the stress orientations throughout the Scotia plate, a finite element mesh was constructed of 599 constant-strain quadrangular elements of eight nodes with a medium size of $50 \times 50\ km^2$. The kinematics and geometry of the main geological structures of the Scotia plate were considered. The model geometry represents the shape of the main Scotia plate boundaries. A heterogeneous elastic rheology was used (Young's modulus = 70 GPa for the oceanic lithosphere, 55 GPa for the continental lithosphere; Poisson coefficient = 0.25; Turcotte and Schubert, 2002). The main boundary conditions for the predicted stresses in the modeling included the deduced e_{HMAX} directions from the focal mechanism analysis and the plate velocity vectors determined by Pelayo and Wiens (1989). Both conditions were considered surface loads or slip motions on the plate boundaries (Fig. 5a). When the model geometry and mesh elements were defined, different boundary conditions were applied to the limits. Using the previously discussed tectonic regime, three plate boundaries were assumed to be active in the model (i.e. push was applied from these boundaries during modeling): the east Scotia spreading center, the north Scotia ridge, and the northwestern part of the SFZ. In the areas of the north and south Scotia ridge close to the east Scotia spreading center, free movement was allowed. In the southeastern part of the SFZ, a strike–slip movement was applied. Other tectonic forces, including topographic and drag forces, were not considered because the predicted stresses fit well with our observations, and the obtained model represents a satisfactory pattern for the induced stress field from the forces applied. This process of applying different boundary conditions to the limits was repeated until the results of the model fit the observed stress field. The final model is shown in Fig. 5b (to simplify, only the stresses of some finite elements have been plotted). The predicted stress model (nonlithostatic horizontal stresses) is characterized by homogeneous NE–SW compression throughout the Scotia plate with some ENE–WSW deflections in the central area and at some borders. At the north and south Scotia ridges, the calculated maximum horizontal stress orientation (S_{HMAX}) is oriented NNE–SSW to ENE–WSW; that is, it lies oblique to the trend of the ridges, which agrees with the proposed left-lateral movement at these boundaries. Between the central region and the southeastern tip of the SFZ, the calculated S_{HMAX} orientations are perpendicular to the SFZ trend. Toward the northwestern tip of the SFZ, S_{HMAX} lies at a steep angle to the trend of the zone. Consequently, the S_{HMAX} orientations along this plate boundary indicate that, at present, this structure could represent an incipient convergent plate boundary. The E–W S_{HMAX} orientation in the east Scotia spreading center is not supported by the focal mechanism data. However, it can be understood as adequate because, for much of their length, the ridge crest and the magnetic lineations from the western flank of the ridge trend N–S (Barker, 2001).

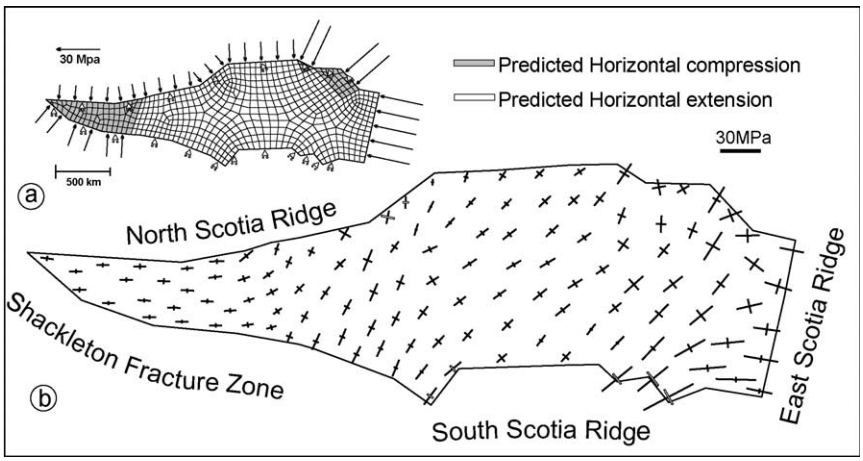

Fig. 5. (a) Scotia plate mesh and boundary conditions for the finite element model (UTM projection). Shaded elements represent the continental lithosphere, and white elements indicate the oceanic lithosphere. Arrows show the surface force loads applied to the model boundaries, and triangles indicate the movement orientations of each boundary (parallel to the base of the triangle). (b) Stresses predicted on the Scotia plate by finite element modeling. Bars indicate the orientation and magnitude of the maximum and minimum horizontal nonlithostatic stresses.

Finally, the computed S_{HMAX} orientations and the e_{HMAX} deduced from focal mechanisms show excellent agreement, which implies that the proposed model is valid (see rose diagrams from Fig. 4). Furthermore, the proposed stress model with the contour parameters described previously also produces extensional stresses in the areas of the Scotia plate where the focal mechanisms agree with an extensional tectonic regime (Zones A2, B1, B2; Fig. 4).

5. Discussion

Fault population analysis of 57 earthquake focal mechanisms located in the Scotia plate region shows a regional NE–SW maximum horizontal shortening (e_{HMAX}); the results are similar for both the slip model and the right dihedra method (Fig. 6). The NE–SW direction coincides with the orientation of slip vectors

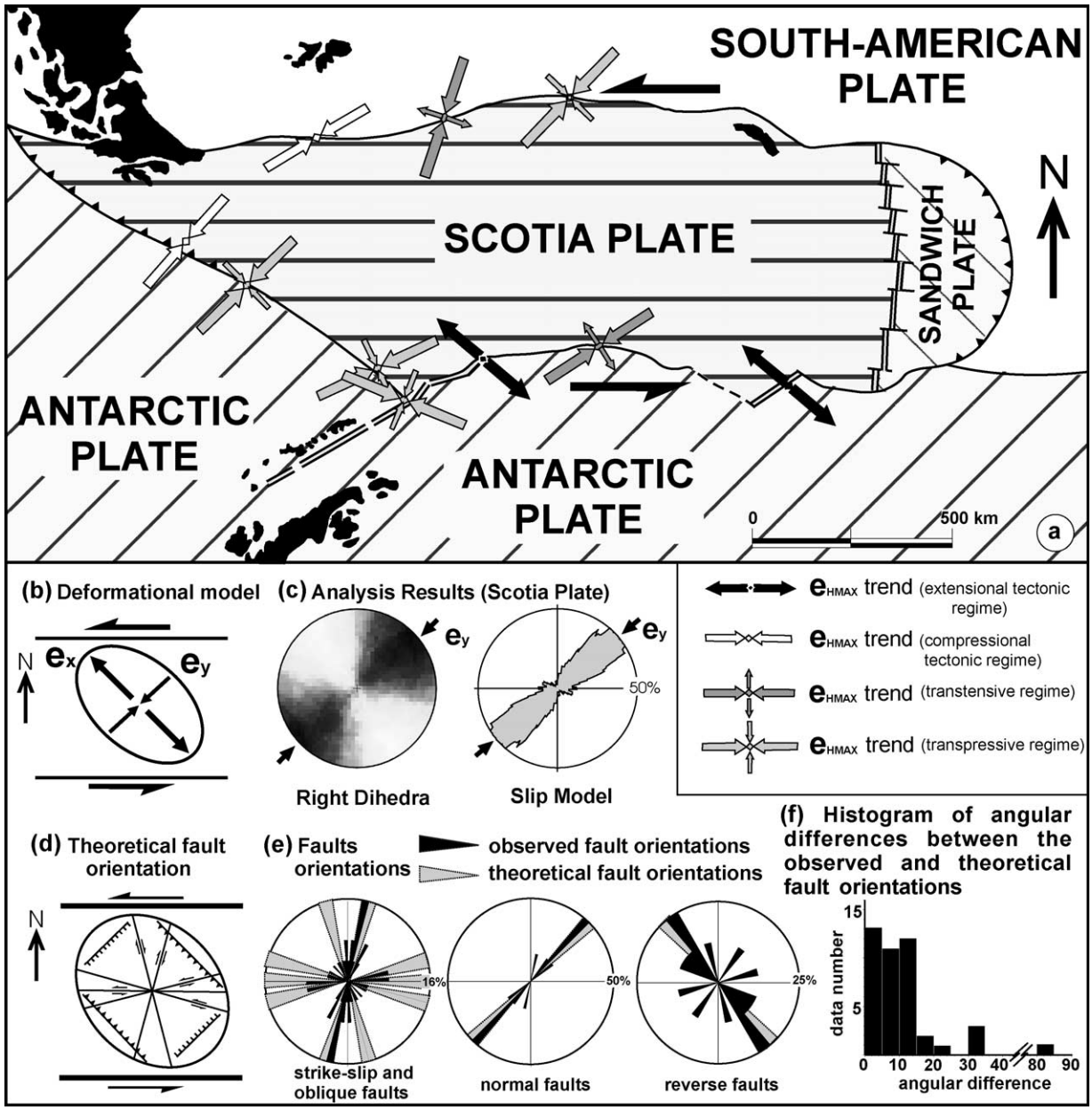

Fig. 6. (a) Schematic representation of the main plate boundaries located in the Scotia plate zone, with the maximum horizontal shortening orientations (e_y) determined from the analysis of earthquakes in the Scotia plate and its limits. The established e_y orientations for each area are represented by the direction of the arrow; the different arrow types show the type of deformational ellipsoid. (b) Deformational model proposed for the Scotia plate. (c) General right dihedra diagram and rose orientations of e_{HMAX} and e_y obtained from the analysis of seismicity at the boundaries of the Scotia plate. (d) Plan view of the geometric relationships between structures formed during a simple shear deformation history, with shear parallel to Scotia plate E–W boundaries. (e) Orientations of faults determined from focal mechanisms (slip model), grouped by type of fracture (strike–slip faults, normal faults, reverse faults). The intervals in dotted gray show the theoretical orientations of faults predicted by this model with a deviation of $\pm 5°$. (f) Histogram of angular differences between the fault orientations of the analyzed earthquakes and the theoretical orientations of predicted faults from the current model.

calculated for the Scotia plate by Pelayo and Wiens (1989) and agrees with the ENE–WSW pattern of horizontal compressive stresses proposed by Forsyth (1975). These results are consistent with the recent maximum horizontal shortening established for the South Shetland Island region on the basis of a study of neotectonic structures (Galindo-Zaldivar et al., 1996; Maldonado et al., 2000).

The Scotia plate is characterized by a leftward motion at its northern and southern boundaries (Fig. 6a). These two boundaries confer a sinistral strike–slip movement in a transpressive tectonic regime on the whole Scotia plate. According to classical shear zone deformation, for a region bounded by two structures with strike–slip movement, the orientation of the maximum extension (e_x) is oblique to the boundaries that produce this direction of motion (Fig. 6b). The angle between the maximum shortening (e_y) and the boundary varies on the basis of whether the realm is transpressional ($<45°$) or transtensional ($>45°$). The theoretical model predicts a maximum horizontal shortening (e_y) trending NE–SW; the e_{HMAX} trend calculated by focal mechanism analysis fits this orientation exactly (the mean e_{HMAX} trend is N48°E, Fig. 6c). This orientation is also predicted in the finite element model (Fig. 5).

According to the proposed shear model (Fig. 6b), faults developed in association with the left-lateral, simple shear coupling of the entire Scotia plate must be located at the position shown in Fig. 6d. Considering the E–W orientation of the plate limits, the normal faults must be oriented close to N45°E, the reverse faults close to N135°E, and the strike–slip faults around five sets close to N15°E, N90°E, N75°E, N115°E, and N165°E (fault orientation according to the theoretical model in Fig. 6d). When the fault orientations deduced from the focal mechanisms are classified according to their slip direction, 83% coincide with those predicted by the theoretical model (Fig. 6e, f). Furthermore, those orientations that do not coincide with the model correspond to earthquakes located outside the Scotia plate in the SW corner near Elephant Island (Zone C; Fig. 2), where other tectonic processes related to rifting in the Bransfield Strait are superimposed (González-Casado et al., 2000).

Finally, it should also be noted that many of the tectonic structures with associated seismicity in the Scotia plate are oriented in the directions predicted by the theoretical shear model. For example, the theoretical reverse fault orientations coincide with the northwestern part of the SFZ (Fig. 1), and the theoretical dip-slip fault orientations coincide with the normal faults or small pull-apart basins located along the east south Scotia ridge zone (Fig. 1). Epicenters inside the Scotia plate are located near old tectonic structures previously considered inactive (Fig. 1). However, the orientations of these structures coincide in trend with the strike–slip fault orientations predicted by the shear model for the entire Scotia plate (e.g. the Quest fracture zone, the Endurance fracture zone, old transform faults of the west Scotia ridge; Fig. 1). Therefore, these old transforming faults may be active strike–slip faults (Fig. 6d).

From a geodynamic point of view, the entire Scotia plate is under a homogeneous deformation regime characterized by NE–SW maximum horizontal shortening (e_y) and NW–SE maximum horizontal extension (e_x) (Fig. 6b). This deformation is induced by the left-lateral movement of the Scotia plate's northern and southern boundaries, which generates a shear couple in the entire plate. The plate geometry and proposed shear model predict that the active faults inside this plate must have the following orientations: normal faults N45°E; reverse faults N135°E; and strike–slip faults N15°E, N90°E, N75°E, N115°E, and N165°E (Fig. 6d). These orientations correspond precisely to those found in the fault orientation deduced from the focal mechanisms, which suggests the proposed model is accurate.

According to the proposed model and previous geophysical and geological studies of the plate boundaries, the proposed stresses produce seismically active reverse and strike–slip faults (north Scotia ridge), normal and strike–slip faults (south Scotia ridge), and reverse and strike–slip faults (SFZ). In the Scotia plate, the seismicity appears related to former structures (the Endurance and Quest fracture zones, Fig.1) that, according to the proposed stress model, must move as strike–slip faults. Only in the SW part of the Scotia plate do the structures and focal mechanism fail to correspond to the proposed model. This is probably due to the interference of other tectonic processes, such as the opening of the Bransfield basin.

The construction of a simple finite element model to study the orientation of the stress field in the Scotia plate allows compressional and extensional trajectories-deduced from earthquake focal mechanism analysis-to be reproduced. The finite element model (Fig. 5) shows very regular e_y trajectories in the Scotia plate with only minor perturbations. Therefore, despite the important tectonic differences among some parts of the Scotia plate, its processes and tectonic structures can be explained by the proposed kinematic model of left-lateral couple shear throughout the entire plate.

Acknowledgements

We thank S. Robertson, A.M. Pelayo, and Prof. J. Kellogg for constructive reviews that helped us improve the quality of the manuscript. Financial support for this work was provided by Spanish Government DCICYT grants ANT98-0225 and MCyT-BTE2002-01742. We also thank A. Burton for improving the English.

References

Acosta, J., Uchupi, E., 1996. Transtensional tectonics along the south Scotia Ridge, Antarctica. Tectonophysics 267, 31–56.

Angelier, J., Mechler, P., 1977. Sur une méthode graphique de recherche des contraintes principales également utilisable en tectonique et sismologie: la méthode des dièdres droits. Bulletin de la Société Géologique de la France 7, 1309–1318.

Bergerat, F., Angelier, J., 2000. The South Iceland Seismic Zone: tectonic and seismotectonic analyses revealing the evolution from rifting to transform motion. Journal of Geodynamics 29, 211–231.

Barker, P.F., 1970. Plate tectonics of the Scotia Sea region. Nature 228, 1293–1296.

Barker, P.F., 1995. Tectonic framework of the East Scotia Sea. In: Taylor, B., (Ed.), Backarc Basins: Tectonics and Magmatism, Plenum Press, New York, pp. 281–314.

Barker, P.F., 2001. Scotia Sea tectonic evolution: implications for mantle flow and palaeocirculation. Earth-Science Reviews 55, 1–39.

Barker, P.F., Burrell, J., 1977. The opening of Drake passage. Marine Geology 25, 15–34.

Barker, P.F., Dalziel, I.W., 1983. Progress in geodynamics in the Scotia Arc region. In: Cabre, R., (Ed.), Geodynamics of the Eastern Pacific Region, Caribbean and Scotia Arcs, American Geophysical Union, Washington, DC, pp. 137–170.

Barker, P.F., Dalziel, I.W., Storey, B.C., 1991. Tectonic development of the Scotia Arc region. In: Tingey, R.J., (Ed.), The Geology of Antarctica, Oxford University Press, New York, pp. 215–248.

Capote, R., De Vicente, González-Casado, J.M., 1991. An application of the slip model of brittle deformations to focal mechanism analysis in three different plate tectonics situations. Tectonophysics 191, 339–409.

Cloetingh, S., Wortel, M.J.R., 1986. Stress in the Indo-Australian plate. Tectonophysics 132, 49–67.

Coblentz, D.D., Sandiford, M., Richardson, R.R., Zhou, S., Hillis, R., 1995. The origins of the intraplate stress field in the continental Australia. Earth and Planetary Science Letters 133, 299–309.

Coblentz, D.D., Zhou, S., Hillis, R.R., Richardson, R.M., Sandiford, M., 1998. Topography, boundary forces and the Indo-Australian intraplate stress field. Journal of Geophysical Research 103, 919–931.

Cunninghan, A.P., Barker, P.F., Tomlinson, J.S., 1998. Tectonics and sedimentary environment of the North Scotia Ridge region revealed by side-scan sonar. Journal of Geological Society, London 155, 941–956.

De Vicente, G., 1988. Análisis poblacional de Fallas. El sector de enlace Sistema Central Español-Cordillera Ibérica. PhD Thesis. Universidad Complutense de Madrid, Spain

De Vicente, G., Giner-Robles, J.L., Muñoz-Martín, A., González-Casado, J.M., Lindo, R., 1996. Determination of present-day tensor and neotectonic interval in the Spanish Central System and Madrid Basin, central Spain. Tectonophysics 266, 405–424.

Dziewonski, A.M., Chou, T.A., Woodhouse, J.H., 1981. Determination of earthquake source parameters from waveform data for studies of global and regional seismicity. Journal of Geophysical Research 86, 2825–2852.

Dziewonski, A.M., Woodhouse, J.H., 1983. An experiment in the systematic study of global seismicity: Centroid-moment solutions for 201 moderate and large earthquakes of 1981. Journal of Geophysical Research 88, 3247–3271.

Engdahl, E.R., Van der Hilst, R.D., Buland, R.P., 1988. Global teleseismic earthquake relocation with improved travel times and procedures for depth determination. Bulletin Seismological Society American 88, 722–743.

Forsyth, D.W., 1975. Fault plane solutions and tectonics of the South Atlantic and Scotia Sea. Geophysical Journal International 80, 1429–1443.

Galindo-Zaldivar, J., Jabaloy, A., Maldonado, A., Sanz de Galdeano, C., 1994. Transtensional deformation and internal basin evolution in the South Scotia Ridge. Terra Antarctica 1, 303–306.

Galindo-Zaldivar, J., Jabaloy, A., Maldonado, A., Sanz de Galdeano, C., 1996. Continental fragmentation along the South Scotia Ridge transcurrent plate boundary (NE Antarctic Peninsula). Tectonophysics 258, 275–301.

Gephart, J.W., Forsyth, D.W., 1984. An improved method for determining the regional stress tensor using earthquake focal mechanism data: application to the San Fernando earthquake sequence. Journal of Geophysical Research 89, 9305–9320.

Giner-Robles, J.L., 1996. Análisis Tectónico y sismotectónico en el sector centro-oriental de la Cuenca del Tajo. PhD Thesis. Universidad Complutense de Madrid, Spain

González-Casado, J.M., Giner-Robles, J.L., López-Martínez, J., 2000. Bransfield Basin, Antarctic Peninsula: not a normal backarc basin. Geology 28, 1043–1046.

Gordon, R.G., DeMets, C., Argus, D.F., Stein, S., 1988. Current plate motions. Eos Transactions, American Geophysical Union 69, 1416.

Gràcia, E., Canals, M., Farràn, M., Prieto, M.J., Sorribas, J., GEBRA team, 1996. Morphostructure and evolution of the Central and Eastern Bransfield Basin (NW Antarctic Peninsula). Marine Geophysical Researches 19, 429–448.

Harmsen, S.C., Rogers, A.M., 1986. Interferences about the local stress field from focal mechanisms: applications to earthquakes in the southern Great Basin of Nevada. Bulletin of the Seismological Society of America 76, 1560–1572.

Herraiz, M., De Vicente, G., Lindo, R., Sánchez-Cabañero, J.G., 1996. Seismotectonics of the Sierra Albarrana area (southern Spain) Constraints for a regional model of the Sierra Morena-Guadalquivir Basin limit. Tectonophysics 266, 425–442.

Herraiz, M., De Vicente, G., Lindo-Ñaupari, R., Giner-Robles, J.L., Simón, J.L., González-Casado, J.M., Vadillo, O., Rodríguez-Pascua, M.A., Cicuéndez, J.I., Casas, A., Cabañas, L., Rincón, P., Cortés, A.L., Ramírez, M., Lucini, M., 2000. A new perspective about the recent (Upper Miocene to Quaternary) and present tectonic stress distributions in the Iberian Peninsula. Tectonics 19, 762–786.

Herron, E.M., Bruhn, R., Winslow, M., Chuaqui, L., 1977. Post-Miocene tectonics of the margin of southern Chile. In: Talwani, M., Pitman, W.C. (Eds.), Islands Arcs, Deep Sea Trenches, and Back-Arc Basins, Pitman III, AGU, Washington, DC, pp. 273–284.

Klepeis, K.A., Lawver, L.A., 1996. Tectonics of the Antarctic–Scotia plate boundary near Elephant and Clarence Islands, West Antarctica. Journal of Geophysical Research 101, 20211–20231.

Larter, R.D., Barker, P.F., 1991. Effects of ridge crest-trench interaction on Antarctic–Phoenix spreading: Forces on a young subducting plate. Journal of Geophysical Research 96, 19583–19607.

Livermore, R., McAdoo, D., Marks, K.M., 1994. Scotia Sea tectonics from high-resolution satellite gravity. Earth and Planetary Science Letters 123, 255–268.

Maldonado, A., Larter, R., Aldaya, F., 1994. Forearc tectonic evolution of the South Shetland margin, Antarctica Peninsula. Tectonics 13, 1345–1370.

Maldonado, A., Balanyá, J.C., Barnolas, A., Galindo-Zaldivar, J., Hernández, J., Jabaloy, A., Livermore, R., Martínez-Martínez, J.M., Rodríguez-Fernández, J., Sanz de Galdeano, C., Somoza, L., Suriñach, E., Viseras, C., 2000. Tectonics of an extinct ridge-transform intersection, Drake Passage (Antarctica). Marine Geophysical Researches 21, 43–68.

Meijer, P.Th., Govers, R., Wortel, M.J.R., 1997. Forces controlling the present-day state of stress in the Andes. Earth and Planetary Science Letters 148, 157–170.

Michael, A.J., 1984. Determination of stress from slip data: faults and folds. Journal of Geophysical Research 89, 11517–11526.

Muñoz-Martín, A., Cloetingh, S., De Vicente, G., Andeweg, B., 1998. Finite-element modeling of tertiary paleostress fields in the eastern part of the Tajo Basin (central Spain). Tectonophysics 300, 47–62.

Pelayo, A., Wiens, D.A., 1989. Seismotectonics and relative plate motions in the Scotia Sea region. Journal of Geophysical Research 94, 7293–7320.

Reches, Z., 1983. Faulting of rocks in three-dimensional strain fields, II. Theoretical analysis. Tectonophysics 95, 133–156.

Richardson, R.M., Reding, L., 1991. North American plate dynamics. Journal of Geophysical Research 96, 12201–12223.

Rivera, L.A., Cisternas, A., 1990. Stress tensor and fault plane solutions for a population of earthquakes. Bulletin of the Seismological Society of America 80, 600–614.

Tectonic map of the Scotia Arc, 1985. British Antarctic Survey, BAS [Misc] 3, scale 1:3,000,000. Cambridge

Turcotte, D.L., Schubert, G., 2002. Geodynamics, 2d ed, Cambridge University Press, Cambridge, England, 456 pp.

Zienkiewicz, O.C., Taylor, R.L., 1994. The finite element method, 4th ed, Basic Formulation and Line Problems, Vol. 1. McGraw-Hill, London, 648 pp.